Kent Academic Repository

Full text document (pdf)

Citation for published version

Saines, P.J. and Harcombe, D.R and Welch, P.G and Manuel, P. and Goodwin, A.L (2016) One-dimension magnetic order in the metal–organic framework Tb(HCOO)3. Physical Review B: Condensed Matter and Materials Physics, 94 . ISSN 0163-1829.

DOI

http://doi.org/10.1103/PhysRevB.94.174429

Link to record in KAR

http://kar.kent.ac.uk/58813/

Document Version

Author's Accepted Manuscript

One-dimensional magnetic order in the metal–organic framework Tb(HCOO)$_3$

Daniel R. Harcombe,[1] Philip G. Welch,[1, 2] Pascal Manuel,[2] Paul J. Saines,[3, *] and Andrew L. Goodwin[1]

[1]*Department of Chemistry, University of Oxford, Inorganic Chemistry Laboratory, South Parks Road, Oxford OX1 3QR, U.K.*
[2]*ISIS Facility, Rutherford Appleton Laboratory, Harwell Science and Innovation Campus, Didcot, Oxfordshire OX11 0QX, U.K.*
[3]*School of Physical Sciences, University of Kent, Canterbury CT2 7NH, U.K.*
(Dated: October 28, 2016)

Variable-temperature neutron scattering measurements, reverse Monte Carlo analysis and direct Monte Carlo simulation are used to characterise magnetic order in the metal–organic framework (MOF) Tb(HCOO)$_3$ over the temperature range 100 K to 1.6 K $= T_N$. The magnetic transition at T_N is shown to involve one-dimensional ferromagnetic ordering to a partially-ordered state related to the triangular Ising antiferromagnet and distinct from the canonical "partially-disordered antiferromagnet" model. In this phase, the direction of magnetisation of ferromagnetic chains tends to alternate between neighbouring chains but this alternation is frustrated and is not itself ordered. We suggest the existence of low-dimensional magnetic order in Tb(HCOO)$_3$ is stabilised by the contrasting strength of inter- and intra-chain magnetic coupling, itself a consequence of the underlying MOF architecture. Our results demonstrate how MOFs may provide an attractive if as yet under-explored platform for the realisation and investigation of low-dimensional physics.

Low-dimensional magnets have long provided an important playground for the discovery and exploitation of unconventional physics[1]—from the earliest studies of soliton excitations in CsNiF$_3$ (Refs. 2–4) to contemporary research into quantum information transport in spin-chain compounds.[5] The sensitivity of these systems to small perturbations results in a rich diversity of phase transitions and complex ordering phenomena. For example, the Ising spin-chain compound Ca$_3$Co$_2$O$_6$ exhibits a variety of equilibrium and non-equilibrium states,[6–8] characterised by *e.g.* long-wavelength incommensurate spin density modulations and field-induced magnetisation plateaux reminiscent of Hofstadter fractalisation.[9,10] Arguably the strongest scientific interest from both experimental and theoretical perspectives has always been in the limit of strict 1D order.[11–16] Yet even in canonical systems such as Ca$_3$Co$_2$O$_6$ the divergence of correlation lengths along 1D spin chains is always accompanied by full 3D magnetic order.[8,17] So the realisation and experimental characterisation of genuine partially-ordered low-dimensional magnetic phases remain an important challenge in the field.[18]

It was in this context that we chose to study magnetic order in terbium(III) formate, Tb(HCOO)$_3$. In metal–organic frameworks (MOFs) such as Tb(HCOO)$_3$, magnetically-active transition-metal or rare-earth ions are connected *via* organic ligands to form extended 3D framework structures. Because organic ligands can support superexchange interactions that span a broad energy range, and because framework design allows controlled incorporation of low-dimensional structural motifs (*e.g.* chains, ladders, layers), MOFs are natural candidate hosts for low-dimensional magnetism.[19] Indeed the magnetic response of a number of key MOF families—including formates,[20] oxalates,[21] and succinates[22,23]—can be interpreted in terms of low-dimensional behaviour. However, nearly all of our collective understanding of magnetic order in MOFs is based on indirect experimental techniques, such as magnetic susceptibility, heat capacity, and dielectric constant measurements.[20–24] Tb(HCOO)$_3$ is a notable exception: it is one of the few MOFs for which neutron scattering measurements have been used to characterise magnetic structure within both antiferromagnetic ($T < T_N \simeq 1.6$ K) and paramagnetic ($T = 3$ K) regimes.[25,26]

That Tb(HCOO)$_3$ might harbour an unconventional partially-ordered magnetic state at low T is a possibility suggested by the results of these earlier neutron scattering studies. Within the paramagnetic regime, spin correlations are strongly 1D in nature: chains of Tb^{3+} ions couple ferromagnetically, but neighbouring chains interact only weakly.[26] On cooling below T_N, the magnetic Bragg peaks that emerge in the neutron scattering pattern, indicative of a magnetic phase transition, are subtly broader than the non-magnetic Bragg reflections (see SI) and are accompanied by a substantial diffuse scattering component that is highly structured in reciprocal space and so indicative of strongly correlated disorder.[27] Moreover, the magnetic structures that were proposed on the basis of conventional crystallographic analysis in both Refs. 25 and 26 require a modulation in Tb^{3+} moment that has no obvious physical origin. In the study of disordered (non-magnetic) materials it is recognised that low-dimensional order often gives Bragg-like scattering features, interpretation of which by conventional crystallographic means leads to spurious structural models.[28,29]

In this study, we report a combination of variable-temperature neutron scattering measurement, reverse Monte Carlo (RMC) analysis, and direct Monte Carlo (DMC) simulation of the evolution of magnetic order in Tb(HCOO)$_3$ on cooling from 100 K to 1.6 K. Our key result is that the spin transition at T_N involves 1D ferromagnetic (FM) order along Tb^{3+} spin-chains to give a partially-ordered state equivalent to the triangular Ising antiferromagnet (TIA). In this low-T phase, the direction of chain magnetisation tends to alternate between neighbouring chains but this alternation is frustrated and is not itself ordered. This state—which emerges also in DMC simulations—is distinct from the 3D "partially disordered antiferromagnet" (PDA) model.[11] Its magnetic scattering pattern contains both Bragg-like and structured diffuse features, with the Bragg intensities indistinguishable from those calculated either from the multiple-moment models suggested in previous Rietveld studies or from the PDA model. The existence of a well-defined 1D state in Tb(HCOO)$_3$ distinguishes this system from other spin-chain triangular antifer-

romagnets such as $Ca_3Co_2O_6$,[8,17] $CsNiF_3$,[30,31] and CoV_2O_6[16] and suggests its low-temperature physics may be of particular interest in the study of 1D magnetism.

Under ambient conditions, $Tb(HCOO)_3$ crystallises in the rhombohedral space group $R3m$.[26,32,33] All Tb^{3+} cations are crystallographically equivalent, and are connected by the O atoms of bridging formate ions to form 1D chains that lie coincident with the crystallographic threefold rotation axes [Fig. 1(a)]. The Tb...Tb separation along a given chain is 3.97 Å with the corresponding Tb–O–Tb angle 105.5°—a geometry that favours ferromagnetic coupling and provides a uniaxial crystal field at the Tb^{3+} site (point symmetry $3m$).[26] The chains pack on a perfect triangular lattice with inter-chain separation $a/\sqrt{3} = 6.02$ Å. Extended Tb–OCO–Tb bridges connect neighbouring chains; one end of the formate bridge has a bifurcated coordination, giving two inequivalent Tb...Tb superexchange pathways (distances 6.16 and 6.57 Å) for each pair of chain neighbours [Fig. 1(b)]. There is no experimental evidence for any change in space group symmetry between room temperature and 1.4 K.[26,34,35]

$Tb(HCOO)_3$ orders magnetically on cooling to 1.4–1.6 K.[26,34] Conventional symmetry analysis of the magnetic Bragg scattering observed in this ordered phase identifies $P3m'1$ as the unique magnetic space group; the corresponding magnetic cell has the same size as the nuclear cell, but the rhombohedral centering is lost. Two distinct spin ordering patterns (and their linear combinations) are consistent with the observed magnetic Bragg reflection conditions and intensities. Both cases demand single-ion anisotropy with local moments aligned parallel to the c-axis, both require FM correlations along the Tb chains, and both correspond to antiferromagnetic (AFM) ordering patterns with zero net magnetisation. In one model, one third of the chains has twice the ordered moment of the other two thirds; the magnetisation direction of these two components oppose [Fig. 1(c)]. In the second model, one third of the chains has no ordered moment, and the other two
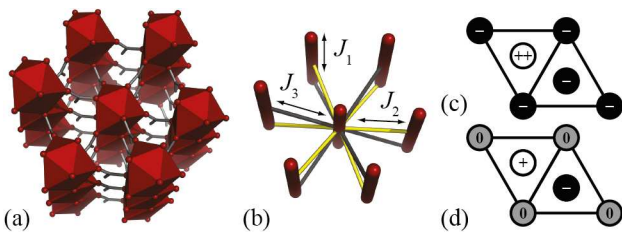
thirds alternate their magnetisation directions [Fig. 1(d)]; in the collinear limit, this describes the average structure of the PDA model.[11] We will come to show that these models are an artefact of applying conventional crystallographic approaches to a state that is not 3D ordered, and that neither model describes the true magnetic structure below T_N.

We study the emergence of magnetic order in $Tb(DCOO)_3$, using variable-temperature (300–1.6 K) neutron powder total scattering data measured by the high-resolution WISH diffractometer at ISIS.[36] Our sample was that reported in Ref. 26; experimental details are given as SI. The final total usable Q-range spanned 0.1–3.7 Å^{-1}, although within this range a total of five regions contaminated with nuclear scattering contributions were excised and omitted from our subsequent analysis. Our corrected data are shown in Fig. 2(a). We found no evidence of magnetic order for $T > 1.6$ K, consistent with the earlier studies of Refs. 26,34.

We fitted these data using the SPINVERT implementation of magnetic RMC,[37,38] applying the analytical approximation to the Tb^{3+} form factor given in Ref. 39 and a linear-in-Q background function.[38] For our initial refinements, we used RMC spin configurations representing a ~$(50$ Å$)^3$ supercell of the nuclear $R3m$ cell (1170 spins, see SI); larger configurations gave equivalent results at greater computational expense. Our SPINVERT fits are shown in Fig. 2(a). The data are well modelled within the paramagnetic regime, with a marginal improvement if we use spins with Heisenberg rather than Ising degrees of freedom (see SI). A SPINVERT fit to the 1.6 K data set—i.e. within the ordered regime—accounts satisfactorily for the diffuse component but cannot reproduce the Bragg scattering [see inset to Fig. 2(a)]. This is to be expected[38] as the reciprocal-space resolution $\Delta Q \sim 0.01$ Å^{-1} required to describe Bragg features is many times smaller than the resolution afforded by our RMC cells ($\Delta Q \simeq 2\pi/r_{max} = 0.2$ Å^{-1}). We will return to this point later in our study.

The temperature dependence of spin orientations and pairwise spin correlations is illustrated in Fig. 2(b) for three representative temperatures (1.7, 2.2, and 8 K). The Ising-like anisotropy noted in Ref. 26 is evident at both 1.7 and 2.2 K, but is not obvious at 8 K. RMC gives a lower bound to the true extent of single-ion anisotropy;[38,40] indeed we cannot rule out that Ising-like behaviour persists to much higher temperatures since RMC fits using Ising spins also provide acceptable fits to the neutron scattering data (see SI). Irrespective of the degree of anisotropy what certainly evolves at low temperatures is the extent of FM correlations along Tb chains. At the very lowest temperatures, AFM inter-chain correlations also become significant, as evidenced by the negative values of $\langle \mathbf{S}(0) \cdot \mathbf{S}(r) \rangle$ for $r = 6.16$ and 6.57 Å. These interactions are necessarily frustrated, and lead to net FM correlations for next-nearest chain neighbours (e.g., $r = a = 10.42$ Å), which are most noticeable at 1.7 K. Spin correlations corresponding to spin pairs taken from chains that are neither nearest neighbours nor next-nearest neighbours are very weak: these account for the series of data points around $\langle \mathbf{S}(0) \cdot \mathbf{S}(r) \rangle = 0$ for $r > 12$ Å.

On the basis of these correlation functions, we anticipated that the basic spin physics of our system might be captured by a combination of Ising-like single-ion anisotropy, FM intra-

FIG. 1: Crystal structure, key magnetic interaction pathways, and candidate magnetic structures of $Tb(HCOO)_3$. (a) Tb^{3+} coordination environments (tricapped trigonal prims; polyhedra) form face-sharing columns parallel to **c**. Columns are arranged on a triangular lattice and are connected by formate ions, shown here in stick representation. (b) Intra-chain exchange pathways are ferromagnetic (J_1), and the two inequivalent inter-chain exchange pathways (J_2, J_3) are collectively antiferromagnetic. Panels (c) and (d) represent the candidate magnetic structures proposed in Refs. 26,34. Circles represent Tb chains projected onto the (a, b) plane, symbols '+' and '−' denote ferromagnetic chains with magnetisations along **c** and −**c**, respectively, and '0' denotes the absence of any ordered moment.
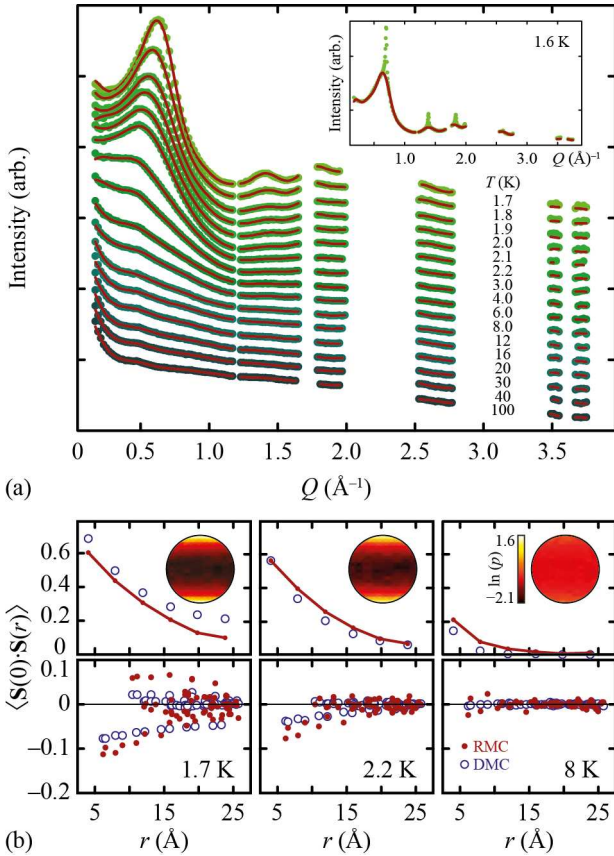
FIG. 2: Temperature-dependent magnetic scattering in Tb(DCOO)$_3$ and its SPINVERT analysis. (a) Scattering data are shown as filled circles, with SPINVERT fits shown as red solid lines. Regions of the scattering pattern contaminated with nuclear scattering have been excluded. The inset shows scattering data collected at 1.6 K within the partially ordered regime together with a small-box SPINVERT fit. (b) Single-ion anisotropy and pairwise correlation functions at three representative temperatures spanning the paramagnetic regime studied here. The single-ion spin orientation functions are shown in stereographic projection, with colours indicating relative distribution probability $p(\theta, \phi) = \rho(\theta, \phi)/\mathrm{d}(\cos\theta)\mathrm{d}\phi$; here $\rho(\theta, \phi)$ is the fraction of total spins within the angular region $\mathrm{d}(\cos\theta)$, $\mathrm{d}\phi$. Spin correlation functions have been separated into intra-chain (top panels) and inter-chain (bottom panels) terms. RMC and DMC results are shown using filled red and open blue circles, respectively; uncertainties are smaller than the symbols.

chain interactions and AFM inter-chain interactions. The simplest Hamiltonian containing these ingredients is

$$\mathcal{H} = J_\parallel \sum_{\langle i,j \rangle} \mathbf{S}_i \cdot \mathbf{S}_j + J_\perp \sum_{\langle\langle i,j \rangle\rangle} \mathbf{S}_i \cdot \mathbf{S}_j - D \sum_i S_{iz}^2, \quad (1)$$

where $\langle \cdots \rangle$ and $\langle\langle \cdots \rangle\rangle$ denote sums over neighbouring spins within and between chains, respectively, $J_\parallel = J_1 < 0$ and $J_\perp = J_2 \equiv J_3 > 0$ are as shown in Fig. 1(b), and $D > 0$ is the single-ion term. To the best of our knowledge, there is no general theory for this interaction model on the rhombohedral lattice that would allow us to extract the J_i, D parameters directly from the experimental spin correlation functions,

even if specific realisations are well understood.[41,42] Consequently, our approach is to use Eq. (1) to drive DMC simulations with different parameter sets to attempt to reproduce the basic temperature dependence of the experimental spin correlation functions, and so identify a set of J_i, D values that capture the key behaviour of paramagnetic Tb(HCOO)$_3$.

Using a grid search approach we tested a variety of candidate J_i, D values, carrying out DMC simulations using the code developed in Ref. 40 and ranking parameter sets according to the fidelity of reproduction of the pairwise spin correlation functions at all measured temperatures. Our DMC spin configurations were the same size and geometry as in the original SPINVERT refinements. Simulations were initialised with random spin orientations, with T systematically lowered from 100 K to 1.7 K following equilibration at each step. Simulations were repeated 100 times and the correlation functions averaged over these independent runs. We found the closest match to experiment for $J_\parallel = -1.5(5)$ K, $J_\perp = 0.03(1)$ K, $D = 70(20)$ K [Fig. 2(b)] (note that we have subsumed the S^2 term within these J_i, D values). While the match to AFM inter-chain interactions is improved by distinguishing J_2 and J_3 (see SI) this effect appears to be marginal. Importantly we do not require this additional complexity for conclusions we draw here as they do not significantly affect the features observed. We do note, however, that the $J_\parallel$ and D parameters showed strong covariance, such that reasonable fits could be obtained with larger $|J_\parallel|$ and smaller D. Because the RMC spin orientation distributions underestimate anisotropy, we cannot use these distributions to help quantify D (other than to act as a flag were the value too low, which is not the case here). Nevertheless the value of D we obtain is consistent with that obtained elsewhere for Tb^{3+} in axial crystal fields,[43] and the qualitative behaviour of the DMC simulations themselves is the same for all acceptable $J_\parallel, D$ combinations we identified (see SI).

As in the real system itself, this particular Hamiltonian exhibits an ordering transition on cooling below $\sim$1.6 K for all J_i, D values consistent with our neutron scattering measurements of the paramagnetic phase (see SI). Direct interrogation of the relevant DMC configurations reveals the low-T state to contain only partial order [Fig. 3(a)]. Individual chains exhibit FM order with their magnetisation aligned either parallel or antiparallel to $\mathbf{c}$; the chain magnetisation tends to alternate between neighbouring chains but this alternation is frustrated by the underlying triangular lattice and so there is no 3D magnetic order. In other words, the state is a realisation of the TIA where individual Ising variables correspond to collective chain magnetisations. We find no evidence of sublattice ordering as implied by the PDA model [Fig. 3(b)]. Extending our TIA model to substantially larger configurations ($ca\ (20\,\mathrm{nm})^3$, or $\sim$10^5 spins) allows calculation of a corresponding neutron scattering pattern of sufficient reciprocal-space resolution to account at once for both Bragg and diffuse scattering. We refined such a model against the experimental data using the SPINVERT code (see SI).[37,38] This process introduced small spin reorientations but preserved the basic TIA spin structure. Crucially, we find that this intermediate order TIA state can account for the entire experimental scattering pattern, includ-
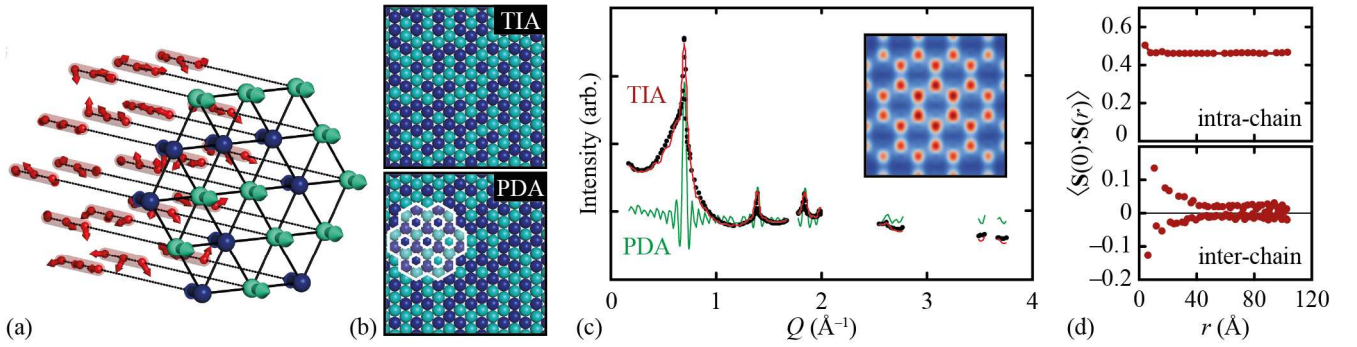
FIG. 3: 1D magnetic order in Tb(HCOO)$_3$. (a) A fragment of the DMC spin configurations at a simulation temperature of 1.5 K is represented in red: spins within a given chain share a common magnetisation direction parallel to the chain axis, with fluctuations away from this vector reflecting the population of spin waves. Projection of these magnetisation directions onto the underlying triangular lattice on which chains are arranged gives a realisation of the TIA (green and blue arrows). (b) Comparison of the TIA and PDA states with Ising variables represented by green and blue spheres. In both cases every triplet of neighbouring Ising states $\epsilon = \pm 1$ obeys the sum rule $|\sum_i \epsilon_i| = 1$, but the PDA model contains a honeycomb sublattice (part of which is shown in white outline) with strict antiferromagnetic order. Sites not included in this sublattice adopt random Ising states; for example, of the seven contained within the highlighted region, five correspond to $\epsilon = -1$ (blue) and two to $\epsilon = +1$ (green). (c) Comparison of experimental neutron scattering data (black symbols) with neutron scattering patterns calculated for Tb(DCOO)$_3$ configurations corresponding to TIA (red line) and PDA (green line) states; the 'ripples' are a finite-size effect[47] and are more noticeable for the PDA model because it contains 3D order. Bragg-like features appear at the regions of reciprocal space associated with maxima in the TIA diffuse scattering pattern (inset). (d) The pairwise spin correlation functions for the TIA model separated into intra-chain (top) and inter-chain (bottom) terms. 1D order has two clear signatures in these correlation functions: the correlation length diverges for intra-chain spin pairs, and the inter-chain correlations vanish as inter-chain separation increases.

ing the appearance of Bragg-like peaks with the correct reflection conditions and relative intensities [Fig. 3(c)]. By construction, this model requires no unphysical modulation of the Tb^{3+} moment. Rather the *magnitude* of chain magnetisation is homogeneous throughout the configuration; our model contains an average spin projection $|\langle S_z \rangle| = 0.662(4)$ along the chain axes with standard deviation = 0.136. A PDA model with the same spin projection values gives a diffraction pattern with the same Bragg reflection conditions and relative Bragg intensities but cannot account for the structured diffuse scattering observed experimentally [Fig. 3(c)]. Hence the TIA model reproduces both the Bragg and diffuse components of the magnetic intensities, but the PDA model accounts only for the Bragg component.

Finally, the spin correlation functions extracted from our TIA configuration reflect the curious coexistence of 1D order and 2D disorder [Fig. 3(d)]. The correlation length diverges (over the ~10 nm scale of our configurations) for *intra*-chain spin pairs, reflecting long-range 1D ferromagnetic order. Because neighbouring (ordered) chains tend to anti-align, the *inter*-chain spin correlations are antiferromagnetic for spin pairs taken from neighbouring chains, and positive for nextnearest chain neighbours. This alternating behaviour continues for spins from successively distant chains, but the magnitude of the spin correlation becomes vanishingly small because there is no long-range magnetic order in the inter-chain directions. The divergence of the 1D ferromagnetic spin correlation length between 1.6 and 1.7 K [*cf* Figs. 2(b) and 3(d)] is consistent with the second-order phase transition postulated on the basis of the analysis of magnetic Bragg scattering using conventional crystallographic approaches.[26] Data collec-

tion at (even) finer temperature intervals around T_N would allow more detailed characterisation of the critical behaviour of this unusual transition.

We now summarise for clarity the various models we have used to arrive at our conclusions regarding the nature of magnetic order in Tb(DCOO)$_3$ at 1.6 K. The key experimental observation we have sought to explain is the bizarre magnetic scattering pattern shown in the inset to Fig. 2(a), which contains a superposition of Bragg-like features and structured diffuse scattering. RMC analysis of these data is computationally intractable because the size of configuration needed to account for the Bragg-like features ($\sim 10^5$ spins) means refinement from a randomly-oriented spin configuration is simply too expensive. DMC simulations allow us to explore phase behaviour at much less expense, and so we have used DMC to generate spin configurations for $T = 1.5\,\mathrm{K} < T_N$, driven by the Hamiltonian in Eq. (1) parameterised so as to match the experimental (RMC) spin correlation functions measured within the paramagnetic regime ($T \geq 1.7\,\mathrm{K}$). At the simulation temperature of 1.5 K, the DMC configuration shows 1D FM order along spin chains but TIA-like disorder between chains; this is the "TIA model" shown in Fig. 3(a,b). We then generated a large spin configuration corresponding to an idealised TIA model, and allowed small spin reorientations during an RMC refinement against the experimental data. The resulting spin configuration accounts entirely for the experimental scattering pattern [Fig. 3(c)]. The spin correlation functions shown in Fig. 3(d) are derived from this RMC-refined TIA model and so represent the experimental spin correlations at 1.6 K. Finally, we verified explicitly that a PDA model (partial 3D order) with intra-chain spin correla-

tions identical to those in our RMC model cannot account for the experimentally-observed diffuse scattering.

So our analysis suggests that the magnetically ordered state of Tb(HCOO)$_3$ accessed below 1.6 K is 1D in nature, such that the remnant spin degrees of freedom map this system onto the 2D TIA. The sharp reflections observed in the neutron scattering patterns are not true Bragg reflections, but correspond to maxima in the continuous scattering function [inset to Fig. 3(c)] with precisely the form expected for TIA phases.[44] It was shown in Ref. 45 that interpretation of these "reflections" using conventional crystallographic approaches leads to a three-sublattice average structure model (*viz.* PDA) as portrayed in Fig. 1(c,d). Consequently, the modulation in magnitude of ordered moment from chain to chain given by that model is an artefact of applying conventional crystallographic tools to a state with no true 3D order.

Our identification of 1D magnetic order in Tb(HCOO)$_3$ has a number of implications. We anticipate by analogy to CsNiF$_3$ the signature of emergent phenomena in its excitation spectrum;[2–4] indeed the contrast in single-ion anisotropy between these two systems (easy-axis *vs* easy-plane) provides a means of testing key aspects of the theory of anisotropic 1D ferromagnets.[1,41] Although Ca$_3$Co$_2$O$_6$ is conceptually similar to Tb(HCOO)$_3$, a distinction between the two is the order-of-magnitude difference in $J_\parallel/J_\perp$ that stabilises the intermediate-order state in the latter.[17] Nevertheless, Tb(HCOO)$_3$ is likely also to show anomalous response to applied magnetic field; indeed magnetisation plateaux may explain its favourable performance as a magnetocaloric material.[16,26] We also anticipate the onset of 3D order at $T \ll J_\perp \sim 30\,\mathrm{mK}$, provided that the transformation kinetics are not prohibitive at such low temperatures. From a materials design perspective, the 1D behaviour of Tb(HCOO)$_3$ is a direct consequence of the underlying MOF architecture. Chemical substitution of formate for longer bridging ligands may allow even more extreme $J_\parallel/J_\perp$ values to be realised, presumably stabilising 1D behaviour over a larger temperature range. Substitution at the Tb^{3+} site may also be of interest:[32] Gd(HCOO)$_3$ exhibits AFM intra-chain coupling, and so the series Gd$_{1-x}$Tb$_x$(HCOO)$_3$ (Ref. 26) may allow realisation of random-chain 1D magnets.[46]

Acknowledgments

* Electronic address: P.Saines@kent.ac.uk
1 M. Steiner, J. Villain, and C. G. Windsor, *Adv. Phys.* **25**, 87 (1976).
2 J. K. Kjems and M. Steiner, *Phys. Rev. Lett.* **41**, 1137 (1978).
3 H. J. Mikeska and M. Steiner, *Adv. Phys.* **40**, 191 (1991).
4 A. P. Ramirez and W. P. Wolf, *Phys. Rev. Lett.* **49**, 227 (1982).
5 S. Sahling, G. Remenyi, C. Paulsen, P. Monceau, V. Saligrama, C. Marin, A. Revcolevschi, L. P. Regnault, S. Raymond, and J. E. Lorenzo, *Nature Phys.* **11**, 255 (2015).
6 S. Aasland, H. Fjelluang, and B. Haubach, *Solid State Commun.* **101**, 187 (1997).
7 A. Maignan, V. Hardy, S. Hébert, M. Drillon, M. R. Lees, O. Petrenko, D. Mc K. Paul, and D. Khomskii, *J. Mater. Chem.* **14**, 1231 (2004).
8 L. C. Chapon, *Phys. Rev. B* **80**, 172405 (2009).
9 H. Kageyama, K. Yoshimura, R. Stern, N. V. Mushnikov, K. Onizuka, M. Kata, K. Kosuge, C. P. Slichter, T. Goto, and Y. Ueda*Phys. Rev. Lett.* **82**, 3168 (1999).
10 S. E. Sebastian, N. Harrison, P. Sengupta, C. D. Batista, S. Francoual, E. Palm, T. Murphy, N. Marcano, H. A. Dabkowska, and B. D. Gaulin, *Proc. Natl. Acad. Sci., U.S.A.* **105**, 20157 (2008).
11 M. Mekata, *J. Phys. Soc. Jpn.* **42**, 76 (1977).
12 N. Motoyama, H. Eisaki, and S. Uchida, *Phys. Rev. Lett.* **76**, 3212 (1996).
13 G. Cao, V. Durairaj, S. Chikara, S. Parkin, and P. Schlottmann, *Phys. Rev. B* **75**, 134402 (2007).
14 R. E. Baumbach, J. J. Hamlin, L. Shu, D. A. Zocco, J. R. O'Brien, P.-C. Ho, and M. B. Maple, *Phys. Rev. Lett.* **105**, 106403 (2010).
15 Y. B. Kudasov, A. S. Korshunov, V. N. Pavlov, and D. A. Maslov, *Phys.-Usp.* **55**, 1169 (2012).
16 M. Nandi and P. Mandal, *J. Appl. Phys.* **119**, 133904 (2016).
17 J. A. M. Paddison, S. Agrestini, M. R. Lees, C. L. Fleck, P. P. Deen, A. L. Goodwin, J. R. Stewart, and O. A. Petrenko, *Phys. Rev. B* **90**, 014411 (2014).
18 C. Coulon, H. Miyasak, and R. Clérac, *Struct. Bond.* **122**, 163 (2006).
19 P. Canepa, Y. J. Chabal, and T. Thonhauser, *Phys. Rev. B* **87**, 094407 (2013).
20 Z. Duan, Z. Wang, and S. Gao, *Dalton Trans.* **40**, 4465 (2011).
21 M. B. Hursthouse, M. E. Light, and D. J. Price, *Angew. Chem. Int. Ed.* **43**, 472 (2004).
22 P. J. Saines, M. Steinmann, J.-C. Tan, H. H.-M. Yeung, W. Li, P. T. Barton, and A. K. Cheetham, *Inorg. Chem.* **51**, 11198 (2012).
23 P. J. Saines, J.-C Tan, H. H.-M. Yeung, P. T. Barton, and A. K. Cheetham, *Dalton Trans.* **41**, 8585 (2012).
24 Y.-G. Huang, F.-L. Jiang, and M.-C. Hong, *Coord. Chem. Rev.* **253**, 2814 (2009).
25 A. I. Kurbakov, J. Rodriguez-Carvajal, V. A. Trounov, and N. V. Starostina, *Mater. Sci. Forum* **321-324**, 971 (2000).
26 P. J. Saines, J. A. M. Paddison, P. M. M. Thygesen, and M. G. Tucker, *Mater. Horiz.* **2**, 528 (2015).
27 D. A. Keen and A. L. Goodwin, *Nature*, **521**, 303 (2015).
28 A. L. Goodwin, M. T. Dove, A. M. Chippindale, S. J. Hibble, A. H. Pohl, and A. C. Hannon, *Phys. Rev. B* **80**, 054101 (2009).
29 A. B. Cairns, M. J. Cliffe, J. A. M. Paddison, D. Daisenberger, M. G. Tucker, F.-X. Coudert, and A. L. Goodwin, *Nature Chem.* **8**, 442 (2016).
30 G. Kamieniarz and C. Vanderzande, *Phys. Rev. B* **35**, 3341 (1987).
31 G. M. Wysin and A. R. Bishop, *Phys. Rev. B* **34**, 3377 (1986).
32 R. Bolotovsky, A. P. Bulkin, G. A. Krutov, V. A. Kudryashev, V. A. Trunov, V. A. Ul'yanov, O. Anston, P. Hiismäki, H. Pöyry,

A. Tiitta, A. A. Loshmanov, and N. G. Furmanova, *Solid State Commun.* **76**, 1045 (1990).

[33] G. Lorusso, J. W. Sharples, E. Palacios, O. Roubeau, E. K. Brechin, R. Sessoli, A. Rossin, F. Tuna, E. J. L. McInnes, D. Collison, and M. Evangelisti, *Adv. Mater.* **25**, 4653 (2013).

[34] V. Trounov, E. Tserkovnaya, S. Gavrilov, and S. Vahrushev, *Phys. B* **234-236**, 679 (1997).

[35] M. R. Moura, A. P. Ayala, J. Mendes Filho, I. Guedes, C. W. A. Paschoal, A. G. Leyva, G. Polla, D. Vega, P. K. de Perazzo, and H. Lanza, *J. Raman Spectrosc.* **35**, 159 (2004).

[36] L. C. Chapon, P. Manuel, P. G. Radaelli, C. Benson, L. Perrott, S. Ansell, N. J. Rhodes, D. Raspino, D. Duxbury, E. Spill, and J. Norris, *Neutron News* **22**, 22 (2011).

[37] J. A. M. Paddison and A. L. Goodwin, *Phys. Rev. Lett.* **108**, 017204 (2012).

[38] J. A. M. Paddison, J. R. Stewart, and A. L. Goodwin, *J. Phys.: Cond. Matt.* **25**, 454220 (2013).

[39] P. J. Brown, *Magnetic form factors*, chapter 4.4.5, International Tables for Crystallography, vol. C (A. J. C. Wilson, ed.), pp. 391-399 (1995).

[40] J. A. M. Paddison, H. Jacobsen, O. A. Petrenko, M. T. Fernandéz-Díaz, P. P. Deen, and A. L. Goodwin, *Science*, **350**, 179 (2015).

[41] J. M. Loveluck, S. W. Lovesey, and S. Aubry, *J. Phys. C: Solid State Phys.* **8**, 3841 (1975).

[42] K. Sasaki, *Prog. Theor. Phys.* **68**, 1518 (1982).

[43] M. J. P. Gingras, B. C. den Hertog, M. Faucher, J. S. Gardner, S. R. Dunsiger, L. J. Chang, B. D. Gaulin, N. P. Raju, and J. E. Greedan, *Phys. Rev. B* **62**, 6496 (2000).

[44] D. H. Wojtas and R. P. Millane, *Phys. Rev. E* **79**, 041123 (2009).

[45] C. Yoon and R. P. Millane, *J. Opt. Soc. Am. A* **31**, 1416 (2014).

[46] T. N. Nguyen, P. A. Lee, and H.-C. zur Loye, *Science* **271**, 489 (1996).

[47] M. G. Tucker, D. A. Keen, M. T. Dove, A. L. Goodwin, and Q. Hui, *J. Phys.: Cond. Matt.* **19**, 335218 (2007).